REPORT No. 83

INCOMPRESSIBLE JET MIXING IN CONVERGING-DIVERGING AXISYMMETRIC DUCTS

PHILIP G. HILL

December 1965

GAS TURBINE LABORATORY
MASSACHUSETTS INSTITUTE OF TECHNOLOGY
CAMBRIDGE · 39 · MASSACHUSETTS

INCOMPRESSIBLE JET MIXING IN CONVERGING-DIVERGING AXISYMMETRIC DUCTS

by

Philip G. Hill

Under the Sponsorship of:

Office of Naval Research - Power Branch
Contract No. Nonr 3963(07)

Gas Turbine Laboratory

Report Number 83

December 1965

Massachusetts Institute of Technology
Cambridge, Massachusetts

ABSTRACT

A test has been made of the constant-turbulent-Reynolds number hypothesis for a turbulent jet flow in a converging-diverging axisymmetric tube. Using the free turbulent jet as the sole source of data for evaluation of the Reynolds number, and velocity shear distributions, the general ducted flow was predicted with the aid of appropriate similarity relations. Calculated results are compared with the extrensive and consistent data of Hembold; good agreement is observed. It is found that the methods of calculation employed can be considerably simplified without large effect on the calculated results. The existence and extent of zones of recirculation are also discussed.

ACKNOWLEDGEMENTS

The author wishes to record his thanks to Mrs. Joan Kukolich for her computational work, to the Office of Naval Research, United States Navy (and particularly to Mr. J. A. Satkowski) for financial support and encouragement and to the M. I. T. Computation Center for the use of their computer facilities.

TABLE OF CONTENTS

LIST OF FIGURES

NOMENCLATURE

b	width of shear layer (Figure 1)
d	nozzle diame^{+} at exit plane
D	tube diameter
m	total mass flow per unit area (Equation 14)
M	momentum parameter (Equation 15)
P	pressure
P_o	initial stagnation pressure of secondary stream
R	tube radius
R_T	turbulent Reynolds number
U	velocity (Figure 1)
U_j	jet velocity (Figure 1)
U_o	outer stream velocity (Figure 1)
x	axial coordinate (Figure 1)
y	radial coordinate (Figure 1)
α	velocity profile integral (Equation 18)
γ	velocity profile shape parameter (Equation 9)
δ	width of shear layer (Figure 1)
η	y/δ
θ	momentum thickness (Equation 4)
λ	U_o/U_j
ρ	density
τ	shear stress
ν_T	eddy kinematic viscosity
ϕ	velocity profile integrals (Equations 6)
ψ	shear stress integral (Equations 6)

INCOMPRESSIBLE JET MIXING IN CONVERGING-DIVERGING AXISYMMETRIC DUCTS

by

Philip G. Hill

I. INTRODUCTION

A. Constant Turbulent Reynolds Number Hypothesis

Many turbulent shear flows have mean streamline patterns which are qualitatively easy to understand yet are very difficult to predict quantitatively due to uncertainty in the effective turbulent shear stresses. In certain cases, however, these stresses may be estimated quite well by assuming that the turbulent Reynolds number $R_T = \Delta U b/\nu_T$ is constant (ΔU being the difference in mean velocity across the shear layer, b the width of the layer and ν_T the so-called eddy kinematic viscosity). Of course, this is at best a very approximate representation of the effects of the turbulence on the mean motion. However, it is worth considering, both because of its proven usefulness in prediction of mean flows and because of the difficulty of improving upon it, either empirically or theoretically. If the effective value of ν_T is to be deduced either from the measured mean velocity field (and the momentum equation) or from direct hot-wire measurements, it is usually very difficult to discern its lateral or streamwise variations in the scatter of experimental data. Refined measuring techniques may lead to improved accuracy but not without great difficulty. Except for certain very simple cases, e.g. the free jet expanding into a stationary medium, its mean value across the flow field is seldom known within 10%. Of course, a compensating factor is that since it is so difficult to deduce ν_T from the mean velocity field, its value need not be known to high precision in order to predict the velocity field quite well.

In Reference (1) it has been shown that the constant-turbulent-Reynolds number assumption yields quite satisfactory results for jet mixing in constant diameter tubes, both before and after the jet has diffused to the tube wall. The turbulent Reynolds number was evaluated from well-established data on the free jet expanding into a stationary medium. Another case where the constant-turbulent-Reynolds number hypothesis appears to hold quite closely is the turbulent wake in an adverse pressure gradient (Ref. 2). In this case the constant was evaluated from data on the constant-pressure turtulent wake, in which the similar velocity profiles and spreading rates differ somewhat from the corresponding ones for the free jet. The Reynolds number based on shear layer half-width $\Delta U b/\nu_T$ (see Fig. 1) is about 100 for the axisymmetric free jet and only about 23 for the two-dimensional constant-pressure wake. The large difference between these values has been rationalized in terms of the corresponding eddy structures by Townsend[3] and Gartshore[4]. Clauser[5] has shown that in the outer part of the turbulent boundary layer $\nu_T \alpha U\delta^*$ (U being the free-stream velocity and δ^* the boundary layer thickness) so that in this case also the turbulent Reynolds number is apparently constant (at least within 10%).

Mellor[6] has developed similarity solutions for free turbulent shear layers under this hypothesis. There is need for further study of the usefulness and limitations of this approximation and the present paper is devoted to a more severe test of it than for the constant-diameter tube of Reference (1). In this case, the tube is converging-diverging and the pressure gradients imposed on the jet mixing are quite substantial. The study is, however, still restricted to the mixing of streams of equal and constant density and the geometry is taken to be axisymmetric.

B. Free Turbulent Jet

Numerous experimental studies on the axisymmetric free turbulent jet (see Ref. 3, p. 47, for example) have established that a few diameters downstream of the nozzle the velocity profile defined by

$$\frac{U}{U_j} = f(\frac{Y}{\delta}) \tag{1}$$

is essentially constant (U_j being the center-line velocity and δ the jet width). Also it has been found that to a very close approximation $\delta \alpha x$ and $U_j \alpha x^{-1/2}$. These facts and the momentum equation together require (see Ref. 1) that the turbulent shear stress distribution, defined by

$$\frac{\tau}{\rho U_j^2} = g(\frac{Y}{\delta}) \tag{2}$$

must also be constant. These simple results are of considerable importance in relation to more complex flows.

C. Jet Immersed in a Constant-Pressure Secondary Stream

When a jet is immersed in a general secondary stream its velocity profiles cannot, strictly speaking, be self-preserving (except for the special case U_0/U_j = const., which corresponds to $U_0 \alpha x^m$). Referring to Figure 1, the hypothesis

$$\frac{U-U_0}{U_j} = f(\frac{Y}{\delta}) \tag{3}$$

is not generally and strictly compatible with the momentum equation. However, it has been shown (Ref. 1) that within the limitations of the best available experimental data, this fact is unimportant as long as U_j is not less than U_0. If relationships (2) and (3) are assumed, then it may be shown that U_j/U_0 and δ/θ depend only on x/θ, the momentum thickness θ being defined by

$$U_0 \theta^2 = 2\pi \int_0^\infty U(U-U_0)\, y\, dy \tag{4}$$

The solution of the momentum equation for this case is (1)

$$\frac{x}{\theta} = \frac{\theta_1}{\psi\sqrt{2\pi\phi_4}} \left[\frac{\Lambda^{3/2}}{3} + 2\left(\frac{\phi_5}{\phi_4} - \frac{\phi_2}{\phi_1}\right)\Lambda^{1/2} + 2\frac{\phi_5}{\phi_4}\left(\frac{3}{2}\frac{\phi_5}{\phi_4} - \frac{\phi_3}{\phi_1}\right)\Lambda^{-1/2} \right] + \text{const.} \qquad (5)$$

in which

$$\Lambda = \frac{U_0}{U_j} + \frac{\phi_5}{\phi_4} \qquad \phi_4 = \int_0^1 f\eta d\eta$$

$$\phi_1 = \int_0^1 f\eta^2 d\eta \qquad \phi_5 = \int_0^1 f^2\eta d\eta$$

$$\phi_2 = \int_0^1 f^2\eta^2 d\eta \qquad \psi = \int_0^1 \eta\left(\frac{\partial}{\partial\eta}\right)\left(\frac{\tau\eta}{\rho U_j^2}\right) d\eta$$

$$\phi_3 = -\int_0^1 \eta f' \int_0^\eta f\eta_1 d\eta_1 d\eta$$

and $$\eta = \frac{Y}{\delta} \qquad (6)$$

If free jet data is used to evaluate the ϕ's and ψ Equation (5) may be used to provide quite a satisfactory estimate of the mixing of the turbulent jet immersed in a secondary stream. The constant in Equation (5) is evaluated from the condition that $U_0 \to 0$ at $x = 0$, the virtual origin.

D. Concentric Jet in a Cylindrical Duct

When the jet interacts with the tube walls, at least three distinct flow regimes are possible (in addition to the relatively short transition zone 6 or 8 jet nozzle diameters from the exit plane of the nozzle).

1) A region in which the jet is approximately self-preserving and is immersed in a potential outer stream which may be accelerating or decelerating, depending on the shape of the duct and the rate of entrainment of mass into the jet.

2) A possible region in which recirculation occurs, following a deceleration of the outer stream. At the beginning of this zone the "edge" of the jet has not yet diffused to the wall and the secondary fluid recirculates through the jet. The pressure gradient is generally observed to be negligible in this zone.

3) The region downstream of the point (fairly distinct in many cases) at which the jet attaches to the wall. An adverse pressure gradient is generally established but the relatively high shearing forces near the wall tend to accelerate the fluid and terminate a zone of recirculation, had it been present.

In region (1) the jet velocity profile may again be well approximated by

$$\frac{U - U_o}{U_j} = f(\frac{y}{\delta}) \tag{7}$$

in which U_o is now a function of x. Again f is determined from free jet data as is the shear stress distribition

$$\frac{\tau}{\rho U_j^2} = g(\frac{y}{\delta}) \tag{8}$$

These relations are also assumed to hold in the recirculation region (2) in which, additionally, the pressure gradient is assumed zero.

In region (3) the jet velocity profile is allowed to change shape according to

$$\frac{U - U_o}{U_j} = f_o(\eta) + \gamma f_1(\eta) \tag{9}$$

in which $\eta = y/R$, f_o is the free jet distribution, $\gamma = \gamma(x)$ and f_1 is a function which satisfies the conditions

$$\eta = 0 \qquad f_1 = f_1' = 0$$

$$\eta = 1 \qquad f_1 = f_1' = 0$$

As far as may be inferred from typical data on velocity profiles, the function

$$f_1(\eta) = \eta^2(1 - \eta)^2 \tag{10}$$

is a satisfactory approximation. The relative un-importance of f_1 is discussed later in the paper.

In spite of the changing shape of the velocity profile in region (3)

the constant turbulent Reynolds number assumption may be retained with, as will be shown, apparently reasonable success. The shear stresses can thus be computed from

$$\tau = \nu_T \rho \frac{\partial U}{\partial y} \tag{11}$$

using the result obtained from the free jet

$$R_T = \frac{U_j R}{\nu_T} = 147 \qquad \left(\text{i.e. } \frac{U_j b}{\nu_T} = 102\right)$$

in which the tube radius R has now replaced the jet half-width.

In general, wall friction is of second order importance in jet mixing problems so that it may be adequately taken into account by supposing that the wall shear stress τ_o can be estimated by

$$\tau_o = C_f\left(\frac{1}{2} \rho U_o^2\right) \tag{12}$$

in which C_f is a constant of the order of 0.005. When the tube diameter is constant the wall shear stress has virtually no influence in those flows where the pressure rise due to jet mixing is significant (in these cases U_o is generally quite small). If the duct converges in the region of jet mixing then U_o can become large enough to make the effects of the wall shear τ_o felt significantly by the stream as a whole.

With the relationships described above, the flow of jets in axisymmetric ducts of general shape can be readily calculated. If the jet nozzle diameter is reasonably small compared to the inlet diameter of the duct, then the jet can be replaced conceptually by a point source in the exit plane of the nozzle. The inlet flow conditions can then be characterized (1) by a single dimensionless flow variable

$$\frac{m}{(M_D)^{1/2}} = \frac{\lambda_o + (d/D)^2}{\sqrt{\lambda_o^2 + 2(1 + 2\lambda_o)(d/D)^2}} \tag{13}$$

in which m is total mass flow per unit area at the duct inlet and is defined by

$$m = \rho U_j \left[\lambda_o + \left(\frac{d}{D}\right)^2\right] \tag{14}$$

where λ_o is the ratio U_o/U_j at the nozzle inlet plane and d/D is the ratio of nozzle and duct diameters at the inlet plane. M is twice the sum of the total momentum pressure forces in the inlet plane. It is given by

$$M = \rho U_j^2 \left[\lambda_o^2 + 2\,(1 + 2\lambda_o)\left(\frac{d}{D}\right)^2\right] \tag{15}$$

Possible values of $\frac{m}{\sqrt{M\rho}}$ lie between 0 and 1.0. For values of $\frac{m}{\sqrt{M\rho}}$ approaching unity, the duct walls have no noticeable effect on the jet mixing; this is the case of a "small" jet mixing with a "large" secondary stream. Small values of $\frac{m}{\sqrt{M\rho}}$ on the other hand signify that the wall effects are important; if $\frac{m}{\sqrt{M\rho}}$ = 0 the net mass flow is zero and the jet nozzle exhausts into a tube whose end is closed.

The appropriate relationship of the dimensionless variables for the flow may be expressed as

$$\frac{U_j}{\sqrt{M/\rho}}, \frac{U_o}{\sqrt{M/\rho}}, \frac{\delta}{R_o}, \gamma, \frac{P - P_o}{M} = f\left(\frac{x}{R_o}, \frac{R}{R_o}, \frac{m}{\sqrt{M\rho}}\right) \tag{16}$$

in which δ, U_j, U_o and x are defined in Figure 1. R is the local duct radius and R_o the initial value. Up to the point of jet attachment to the wall $\gamma = 0$ and past this point δ is no longer a variable (the shear layer has then constant width and its velocity profile changes shape with alteration in γ). The quantities $\frac{m}{\sqrt{M\rho}}$, m and M are defined in Equations 13, 14 and 15 and P_o is the stagnation pressure of the secondary stream at the inlet plane.

E. Purpose of the Present Paper

The object of this paper is to demonstrate that the simple approximations outlined above have quantitative value in predicting the flow in converging-diverging axisymmetric ducts. The physical approximations are quite severe,

especially in the zone of recirculation, but it will be seen by comparison with extensive experimental data of Hembold (7) and Curtet (8) that over a wide range of flows, the prediction is surprisingly good, especially when corrections are made for the effects of wall friction.

II. METHODS OF CALCULATION

A. Upstream of Jet Attachment

In this zone the four variables that are to be determined by integral techniques are U_j, $\lambda = U_o/U_j$, δ, and p, the pressure. They are determined by using an integral form of the continuity equation, and three integrals of the momentum equation of the form

$$\int_0^R \left(U \frac{\partial U}{\partial x} + V \frac{\partial V}{\partial y} + \frac{1}{\rho} \frac{\partial P}{\partial x}\right) y^i \, dy = \int_0^R \frac{1}{y} \frac{\partial}{\partial y} \left(\frac{\tau}{\rho} y\right) y^i \, dy \qquad (17)$$

$$i = 1, 2, 3$$

Equation (7) is used for the velocity U, the distribution function f being evaluated directly from free-jet data (1). The pressure $P = \overline{p + \rho u'^2}$ is assumed constant across the test section. In the jet ($0 \leq y \leq \delta$) the shear is obtained from an integral of Equation (8) again using free-jet data (1) for numerical evaluations. Outside the jet ($\delta \leq y < R$) the flow is assumed shearless except for a concentrated shear force τ_o applied at the wall. By these steps the continuity equation and the three momentum integral equations can be expressed as in the coefficient matrix of Table I. In the first row of Table I the primes denote differentiation with respect to x/R_o and the variables U_j, δ, R and P indicate the dimensionless variables of relationship (16). λ is the velocity ration U_o/U_j. In the region of recirculation ($U_o < o$), the pressure gradient is set equal to zero, and the last equation is not used.

The coefficients appearing in Table I are defined as follows and

evaluated in Table II.

$$i = 1, 2, 3$$

$$\alpha_{0i} = 2\int_0^1 f\eta^i d\eta \qquad \alpha_{6i} = -\int_0^1 f'\eta^{i-1}\int_0^\eta g\zeta d\zeta d\eta$$

$$\alpha_{1i} = 2\int_0^1 g\eta^i d\eta \qquad \alpha_{7i} = -\int_0^1 g'\eta^{i-1}\int_0^\eta f\zeta d\zeta d\eta$$

$$\alpha_{2i} = \int_0^1 f^2\eta^i d\eta \qquad \alpha_{8i} = -\int_0^1 g'\eta^{i-1}\int_0^\eta g\zeta d\zeta d\eta$$

$$\alpha_{3i} = 2\int_0^1 fg\eta^i d\eta \qquad \alpha_{9i} = -\int_0^1 f'\eta^i d\eta$$

$$\alpha_{4i} = \int_0^1 g^2\eta^i d\eta \qquad \alpha_{10i} = -\int_0^1 g'\eta^i d\eta$$

$$\alpha_{5i} = -\int_0^1 f'\eta^{i-1}\int_0^\eta f\zeta d\zeta d\eta$$

B. Downstream of Jet Attachment

In this region four equations are needed, and again the integral continuity equation and the three momentum integrals of Equation (16) are used. The difference between this region and the previous is mainly that the jet shear layer now has constant width ($\delta = R$) but is allowed to have a changing velocity profile ($\gamma \neq 0$ in Equation (9)). If backflow occurs, the pressure gradient is not set equal to zero, because in this case the entire flow is subject to shearing stresses.

The four equations may be represented by

$$\beta_{j1}\frac{U_j'}{U_j} + \beta_{j2}\lambda' + \beta_{j3}\lambda' + \beta_{j4}\frac{p'}{U_{10}^2} = \beta_{j5}\left(-\frac{R'}{R}\right) + \frac{\beta_{j6}}{R}$$

in which the coefficients β_{jk} are evaluated from

$$\beta_{jk} = \sigma_{1jk}\lambda^2 + \sigma_{2jk}\lambda + \sigma_{3jk}\lambda\gamma + \sigma_{4jk} + \sigma_{5jk}\gamma + \sigma_{6jk}\gamma^2$$

Finally, the coefficients σ_{ijk} are given in Table III. The coefficients appearing in Table III are obtained from Table II.

III. RESULTS

A. Wall Pressure Distribution

The methods described in Part II have been used to calculate the flow in the axisymmetric channel in which Hembold[7] made careful measurements of the wall pressure distributions, and velocity field. The geometry of his test section is given in Table IV.

Figures 2, 3, and 4 show a comparison of measured and calculated wall pressure distributions for a wide range of inlet conditions ($.162 < m/\sqrt{MP} < .697$). On Figure 2 the relative importance of wall friction is indicated by the two sets of lines corresponding to C_f values of 0 and 0.005. It will be seen that at the highest values of $m/\sqrt{Mp}$, wall friction effects are appreciable, particularly on the downstream side of the contraction.

The value of the turbulent Reynolds number used in these calculations was determined directly from data on the free jet (1) and had the magnitude ($U_j\delta/\nu_T$ or U_jR/ν_T) of 147. This is equivalent to $U_jb/\nu_T = 102$ for the free jet. The velocity profile $f(\eta)$ was deduced directly from free jet measurements. Thus, nothing except free jet data was used in calculating the theoretical results indicated in Figures 2 through 12.

Figure 5, a crossplot of the twelve sets of data for two values of x/D shows a very acceptable consistency in the experimental results. The predicted pressures are generally somewhat higher than the experimental ones. While arbitrary adjustments of R_T and C_f could have been used to bring the calculations into even closer accord with the data, this was not done since the point of the exercise was to see how well this particular flow could have been predicted if nothing except the wall geometry were known in advance.

B. Velocity Field

Figure 6 shows both experimental and calculated velocity distributions for

the one inlet condition ($m/\sqrt{MP}$ = 0.499) for which these data are reported by Hembold. The agreement is relatively good at x/D_o = 0.5 but deteriorates at higher values of x/D_o, suggesting that the velocity profiles employed in the calculation method could be improved upon.

Figure 7 is a crossplot of the dimensionless jet velocity profiles and shows that, as expected, their shapes are practically identical up to x/D = 3.5, which is well ahead of the point at which the jet has spread all the way to the wall. However, it may be noted in Figure 7 the function $f(\eta)$ (deduced from free jet data (1)) somewhat overestimates the velocity at the edge of the jet. Velocities near the edge of a free turbulent jet are of course very difficult to determine accurately.

The calculated widths of the jet before it touches the wall are shown for four values of $m/\sqrt{MP}$ in Figure 8. Experimental points for $m/\sqrt{MP}$ = 0.499 are also shown; these were determined by obtaining b (see Fig. 1) from the velocity profiles and using $\delta = 1.44b$. The third of the experimental points shown actually corresponds to a point downstream of jet attachment.

Figures 9 and 10 show how the calculated values of U_o and U_j (see Fig. 1 for definitions) vary along the tube. The few experimental data points for $m/\sqrt{MP}$ = 0.499 are also indicated. For $m/\sqrt{Mp}$ less than about 0.35 it appears that a recirculation zone is possible.

C. Recirculation

From Figure 11 a comparison can be made of calculated and experimentally determined physical boundaries of recirculation in a constant-diameter tube. The calculations were made with exactly the same procedures as for the foregoing case. The predicted axial length of the recirculation zone is the vertical distance between the top and bottom branches of the solid curve.

Experimentally, Barchilon and Curtet used a bubble injection apparatus

to visualize the zone of recirculation. Also they deduced the mean streamline pattern from hot-wire measurements of mean velocity. It will be noted that their measurements and the present calculation method agree very well on the location of the upstream boundary of recirculation. Surprisingly, however, their measurements* indicated that the location of the downstream boundary is independent of $m/\sqrt{M_0}$. Calculations indicate that the strength of the recirculating eddy is quite strongly dependent on $m/\sqrt{M_0}$. Figure 12 shows, for example, how the maximum intensity of backflow theoretically depends on $m/\sqrt{M_0}$ for the constant-diameter tube., The present calculations have, of course, employed quite severe approximations in treatment of the recirculation zone and it seems clear that further experimental and analytical work is needed in this area.

D. Simplification of the Calculation Method

A major simplification of the calculations described herein can be obtained if the change in shape of the shear zone after the jet touches the wall is ignored. Setting the function γ identically equal to zero means that less than half of the coefficients of Tables II and III are needed, and the momentum equations for the downstream zone are very much reduced in size. The question is whether this further approximation has any serious effect on the accuracy of the prediction method.

Figure 13 shows how the calculated value of γ (see Equation (9)) varies with $m/\sqrt{M_0}$ and x/D. The maximum value of the function $f_1(\eta)$ in the equation

$$U = U_o + U_j [f_o(\eta) + \gamma f_1(\eta)]$$

is 0.0625. Since the maximum value of f_o is unity, Figure 13 indicates that

* They have expressed their results in terms of a parameter C_t to which the present one is related by $m/\sqrt{M_0} = [1 + 2/C_t]$

fairly substantial variations in the shape of the velocity profile are predicted. However, Figure 14 shows that actually the modification in the calculated wall pressure distributions is quite small. Suppressing γ makes the predicted results deviate somewhat further from the experimental ones, but not much. Both in the constant-diameter tube and the variable diameter geometry used by Hembold, effects of the change in velocity profile shape seems quite unimportant.

IV. CONCLUSIONS

A.

The constant-turbulent-Reynolds number hypothesis appears to provide a quite satisfactory description of the velocity field of a jet enclosed in a variable-diameter tube. All empirical data used in the calculation method were evaluated from information on the well-known round free jet.

B.

The method appears to predict the incidence of recirculation very well though the details and extent of this zone of backward flow are probably not adequately treated by the simplified descriptions of the velocity field used in this work. More work is needed to provide satisfactory methods of predicting the mean velocity fields in zones of recirculation.

C.

Although the "jet" part of the velocity profile must depart substantially from a self-preserving shape after the jet spreads to the wall, it is apparently not necessary to take this into account in order to obtain a fairly good estimate of the overall dynamics of the mixing zone, e.g. the static pressure rise.

TABLE I

COEFFICIENT MATRIX FOR FLOW UPSTREAM OF JET ATTACHMENT

COEFFICIENT OF / EQUATION	U'_j/U_j	λ'	δ'/δ	$P'/U_{j_0}^2$	R. H..S.
Continuity	$\lambda + \alpha_{01}(\frac{\delta}{R})^2$	1	$2\alpha_{01}(\frac{\delta}{R})^2$	0	$-2\lambda \frac{R'}{R}$
Momentum Integral (i = 1)	$\frac{\lambda^2}{2}\frac{R}{\delta^2} + \frac{3}{2}\alpha_{01}\lambda + \alpha_{21} + \alpha_{51}$	$\frac{\lambda R^2}{2\delta^2} + \alpha_{01}$	$\alpha_{01}\lambda + 2\alpha_{51}$	$\frac{1}{2U_j^2}(\frac{R}{\delta})^2$	$-\frac{C_f\lambda^2}{2}\frac{R}{\delta^2}$
Moment-of-Momentum Integral (i = 2)	$\frac{\lambda^2}{3}\frac{R}{\delta^3} + \frac{7}{4}\alpha_{02}\lambda + \alpha_{22} + \alpha_{52}$	$\frac{\lambda R^3}{3\delta^3} + \frac{5}{4}\alpha_{02}$	$\frac{3}{2}\alpha_{02}\lambda + 2\alpha_{52}$	$\frac{1}{3U_j^2}(\frac{R}{\delta})^3$	$\frac{1}{R_T}\frac{\alpha_{91}}{\delta} - \frac{C_f\lambda^2}{2}\frac{R^2}{\delta^3}$
Second Moment Equation (i = 3)	$\frac{\lambda^2}{4}\frac{R^4}{\delta^4} + 2\alpha_{03}\lambda + \alpha_{23} + \alpha_{53}$	$\frac{\lambda R^4}{4\delta^4} + \frac{3}{2}\alpha_{03}$	$2\alpha_{03}\lambda + 2\alpha_{53}$	$\frac{1}{4U_j^2}(\frac{R}{\delta})^4$	$\frac{1}{R_T}\frac{\alpha_{92}}{\delta} - \frac{C_f\lambda^2}{2}\frac{R^3}{\delta^4}$

TABLE II

i	1	2	3
α_{0i}	0.190	0.0755	0.0380
α_{1i}	0.0333	0.0191	0.0119
α_{2i}	0.0445	0.0124	0.00449
α_{3i}	0.00798	0.00349	0.00172
α_{4i}	0.000794	0.000433	0.000253
α_{5i}	0.0445	0.0229	0.0135
α_{6i}	0.00400	0.00249	0.00169
α_{7i}	0.00399	0.00380	0.00321
α_{8i}	0.000794	0.000651	0.000530
α_{9i}	0.377	0.190	-
α_{10i}	0.0333	0.0333	-

TABLE III

COEFFICIENT MATRIX FOR FLOW DOWNSTREAM OF JET ATTACHMENT

Equation	j	k	1	2	3	4	5	6
Continuity	1	1	0	$\frac{1}{2}$	0	$\frac{1}{2}\alpha_{01}$	$\frac{1}{2}\alpha_{11}$	0
		2	0	0	0	$\frac{1}{2}$	0	0
		3	0	0	0	$\frac{1}{2}\alpha_{11}$	0	0
		4	0	0	0	0	0	0
		5	0	1	0	α_{01}	α_{11}	0
		6	0	0	0	0	0	0
Moment Integral	2	1	1	$\frac{3}{2}\alpha_{01}$	$\frac{3}{2}\alpha_{11}$	$\alpha_{21} + \alpha_{51}$	$\alpha_{31} + \alpha_{61} + \alpha_{71}$	$\alpha_{41} + \alpha_{81}$
		2	0	$\frac{1}{2}$	0	α_{01}	α_{11}	0
		3	0	$\frac{1}{2}\alpha_{11}$	0	$\frac{1}{2}\alpha_{31} + \alpha_{61}$	$\alpha_{41} + \alpha_{81}$	0
		4	0	0	0	$1/(2U_j^2)$	0	0
		5	0	α_{01}	α_{11}	$2\alpha_{51}$	$2\alpha_{61} + 2\alpha_{71}$	$2\alpha_{81}$
		6	$-\frac{1}{2}C_f$	0	0	0	0	0
Moment of Momentum	3	1	$\frac{1}{3}$	$\frac{7}{4}\alpha_{02}$	$\frac{7}{4}\alpha_{12}$	$\alpha_{22} + \alpha_{52}$	$\alpha_{32} + \alpha_{62} + \alpha_{72}$	$\alpha_{42} + \alpha_{82}$
		2	0	$\frac{1}{3}$	0	$\frac{5}{4}\alpha_{02}$	$\frac{5}{4}\alpha_{12}$	0
		3	0	$\frac{1}{2}\alpha_{12}$	0	$\frac{1}{2}\alpha_{32} + \alpha_{62}$	$\alpha_{42} + \alpha_{82}$	0
		4	0	0	0	$1/(3U_j^2)$	0	0
		5	0	$\frac{3}{2}\alpha_{02}$	$\frac{3}{2}\alpha_{12}$	$2\alpha_{52}$	$2\alpha_{62} + 2\alpha_{72}$	$2\alpha_{82}$
		6	$-\frac{1}{2}C_f$	0	0	α_{91}/R_T	α_{101}/R_T	0
Second Moment	4	1	$\frac{1}{4}$	$2\alpha_{03}$	$2\alpha_{13}$	$\alpha_{23} + \alpha_{53}$	$\alpha_{33} + \alpha_{63} + \alpha_{73}$	$\alpha_{43} + \alpha_{83}$
		2	0	$\frac{1}{4}$	0	$\frac{3}{2}\alpha_{03}$	$\frac{3}{2}\alpha_{13}$	0
		3	0	$\frac{1}{2}\alpha_{13}$	0	$\frac{1}{2}\alpha_{33} + \alpha_{63}$	$\alpha_{43} + \alpha_{83}$	0
		4	0	0	0	$1/(4U_j^2)$	0	0
		5	0	$2\alpha_{03}$	$2\alpha_{13}$	$2\alpha_{53}$	$2\alpha_{63} + 2\alpha_{73}$	$2\alpha_{83}$
		6	$-\frac{1}{2}C_f$	0	0	α_{92}/R_T	$2\alpha_{102}/R_T$	0

TABLE IV

HEMBOLD MIXING TUBE ($\frac{d}{D}$ = 0.10)

Axial Distance From Initial Plane (inches)	Diameter (inches)
.000	6.030
1.245	5.850
2.895	5.670
4.689	5.484
6.591	5.301
8.637	5.118
10.785	4.932
13.095	4.746
15.540	4.560
17.100	4.446
20.100	4.262
23.100	4.141
26.100	4.082
29.100	4.085
32.100	4.151
35.100	4.279
38.100	4.470
41.100	4.723
44.100	5.038
47.100	5.415
50.100	5.855
51.000	6.000

REFERENCES

1. Hill, P. G. - "Turbulent Jets in Ducted Streams" - J. Fluid Mechanics, vol. 22, part 1, pp. 161-186 - 1965.

2. Hill, P. G., U. W. Schaub and Y. Senoo - "Turbulent Wakes in Pressure Gradients" - J. Applied Mechanics, vol. 85, pp. 518-524 - 1963.

3. Gartshore, I. S. - "Jets and Wall Jets in Uniform Streaming Flow" - McGill University, Mechanical Engineering Report No. 64-4 and "The Streamwise Development of Certain Two-Dimensional Shear Flows" - McGill University, Mechanical Engineering Report No. 65-3.

4. Townsend, A. A. - The Structure of Turbulent Shear Flow - Cambridge University Press, Cambridge, England - 1956.

5. Clauser, F. - "The Turbulent Boundary Layer" - Advanced Applied Mechanics, vol. 4, pp. 1-51 - 1956.

6. Mellor, G. - "Linear Jet and Wake Solutions with Pressure Gradients" - AIAA Journal, pp. 975-977 - May 1965.

7. Hembold, H. B., G. Luessen and A. M. Heinrich - "An Experimental Comparison of Constant Pressure and Constant Diameter Jet Pumps" - University of Wichita, School of Engineering, Engineering Report No. 147 - 1954.

8. Barchilon, M. and R. Curtet - "Some Details of the Structure of an Axisymmetric Confined Jet with Back Flow" - ASME paper 64-FE-23 - presented at the Fluids Engineering Conference, Philadelphia, Pa. - May 18-21, 1964.

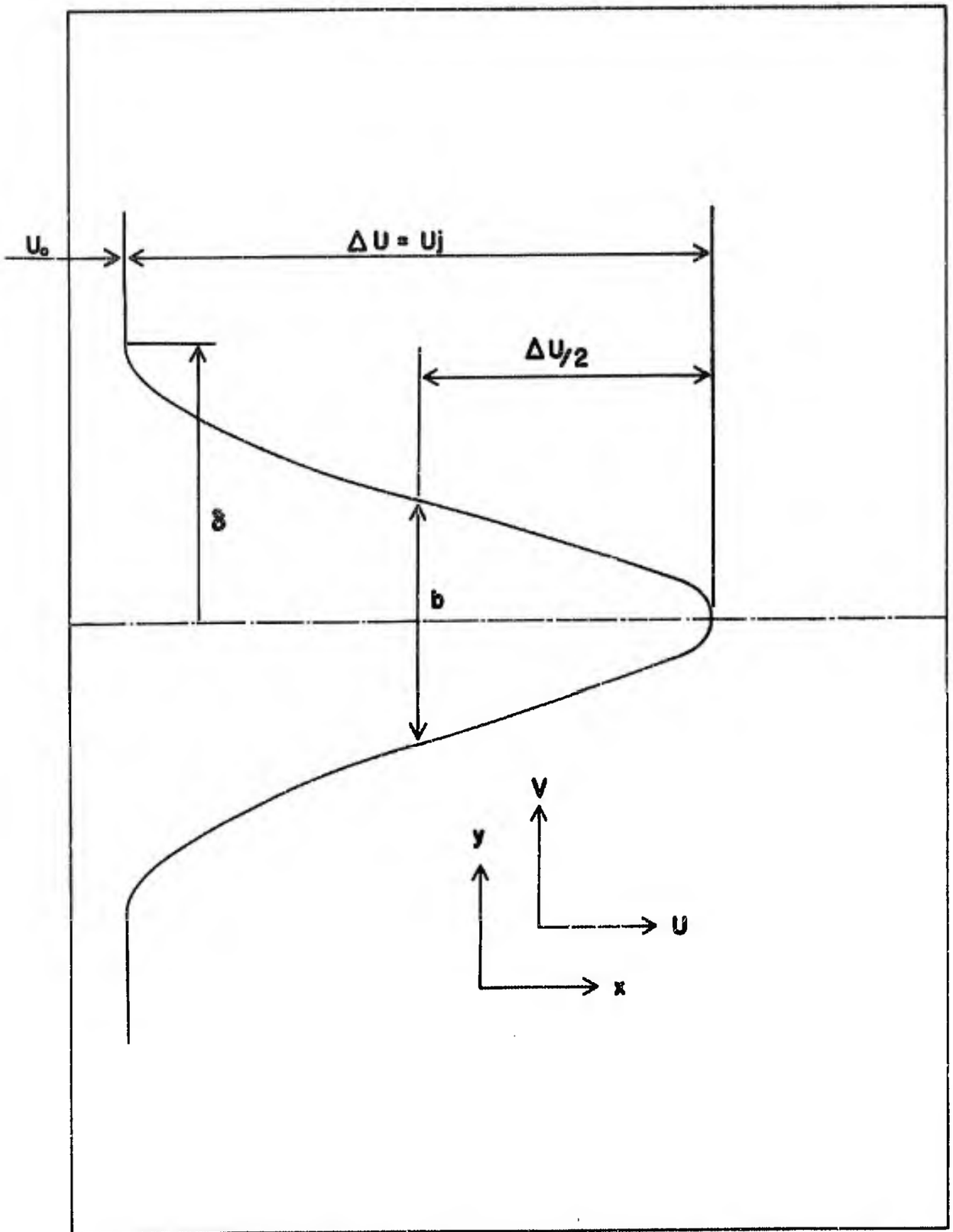

DEFINITIONS OF THE VELOCITY PROFILE FIGURE 1

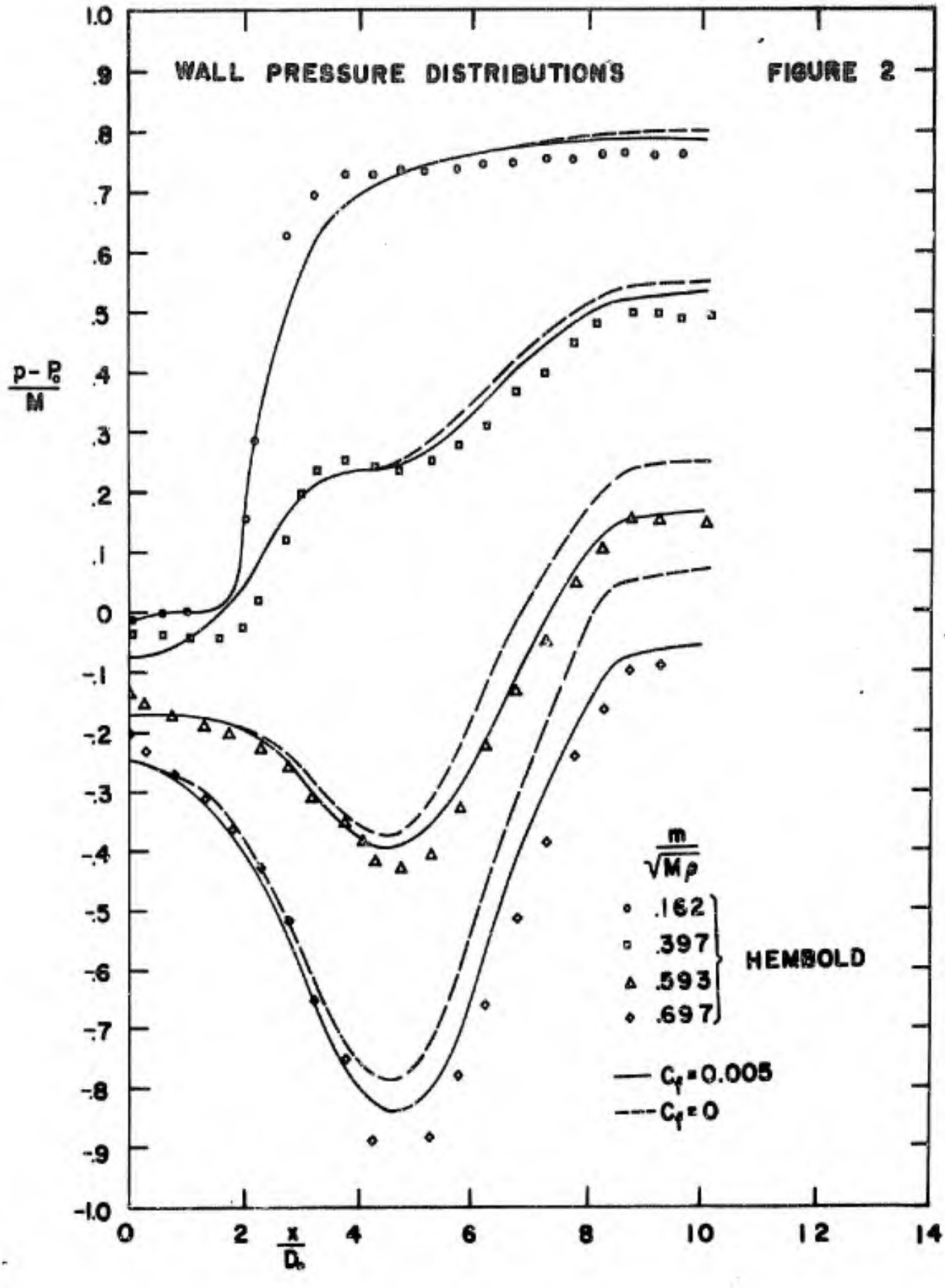
WALL PRESSURE DISTRIBUTIONS
FIGURE 2
$\frac{p-p_0}{M}$
$\frac{x}{D_0}$
$\frac{m}{\sqrt{Mp}}$
.162
.397
.593
.697
HEMBOLD
$C_f = 0.005$
$C_f = 0$

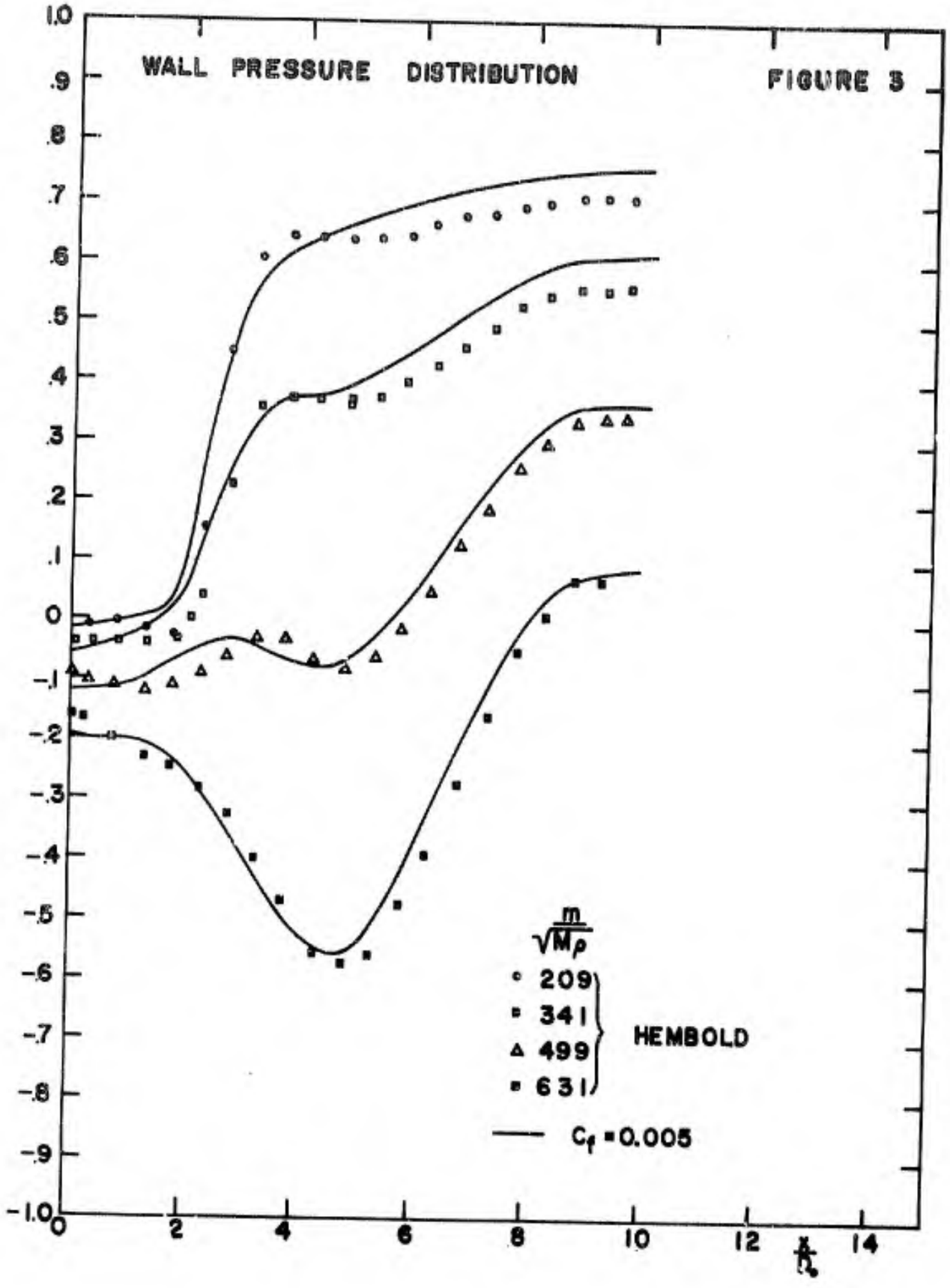
WALL PRESSURE DISTRIBUTION
FIGURE 3
1.0
.9
.8
.7
.6
.5
.4
.3
.2
.1
0
-.1
-.2
-.3
-.4
-.5
-.6
-.7
-.8
-.9
-1.0
0
2
4
6
8
10
12
14
x/L
m/√Mρ
209
341
499
631
HEMBOLD
Cf = 0.005

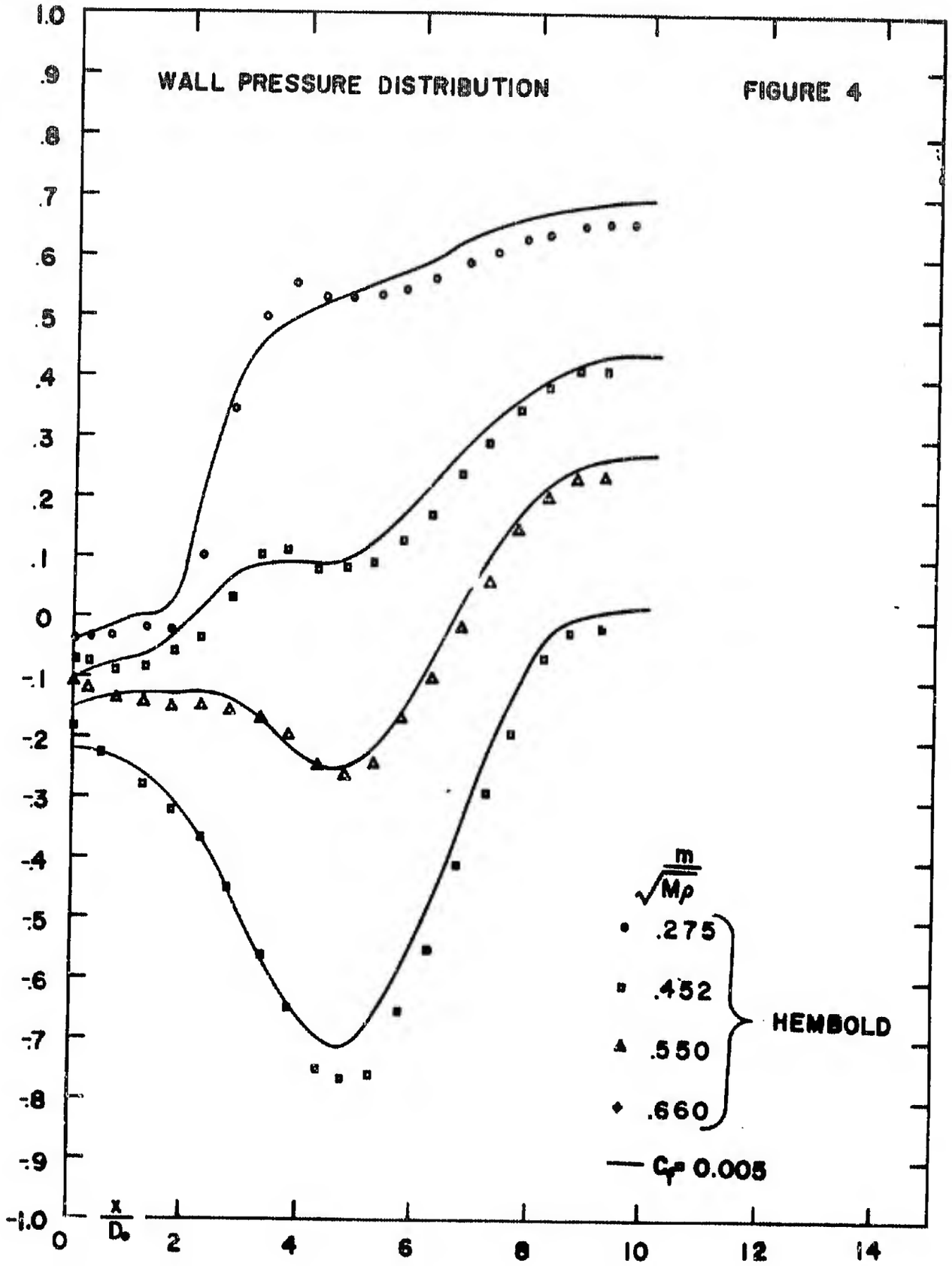
WALL PRESSURE DISTRIBUTION
FIGURE 4
1.0
.9
.8
.7
.6
.5
.4
.3
.2
.1
0
-.1
-.2
-.3
-.4
-.5
-.6
-.7
-.8
-.9
-1.0
0
2
4
6
8
10
12
14
x/D
m/√Mρ
.275
.452
.550
.660
HEMBOLD
Cf = 0.005

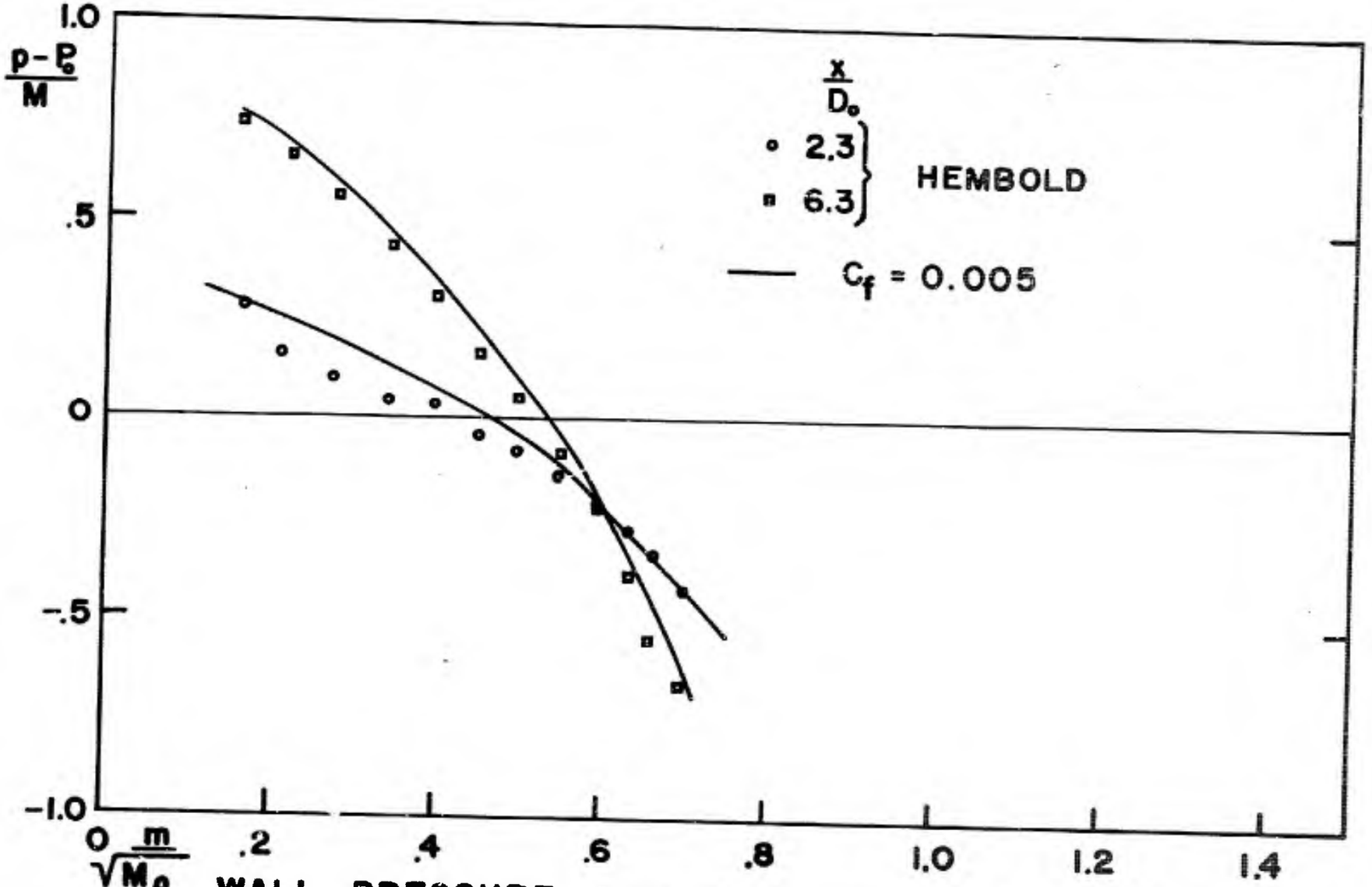

WALL PRESSURE DISTRIBUTIONS FIGURE 5

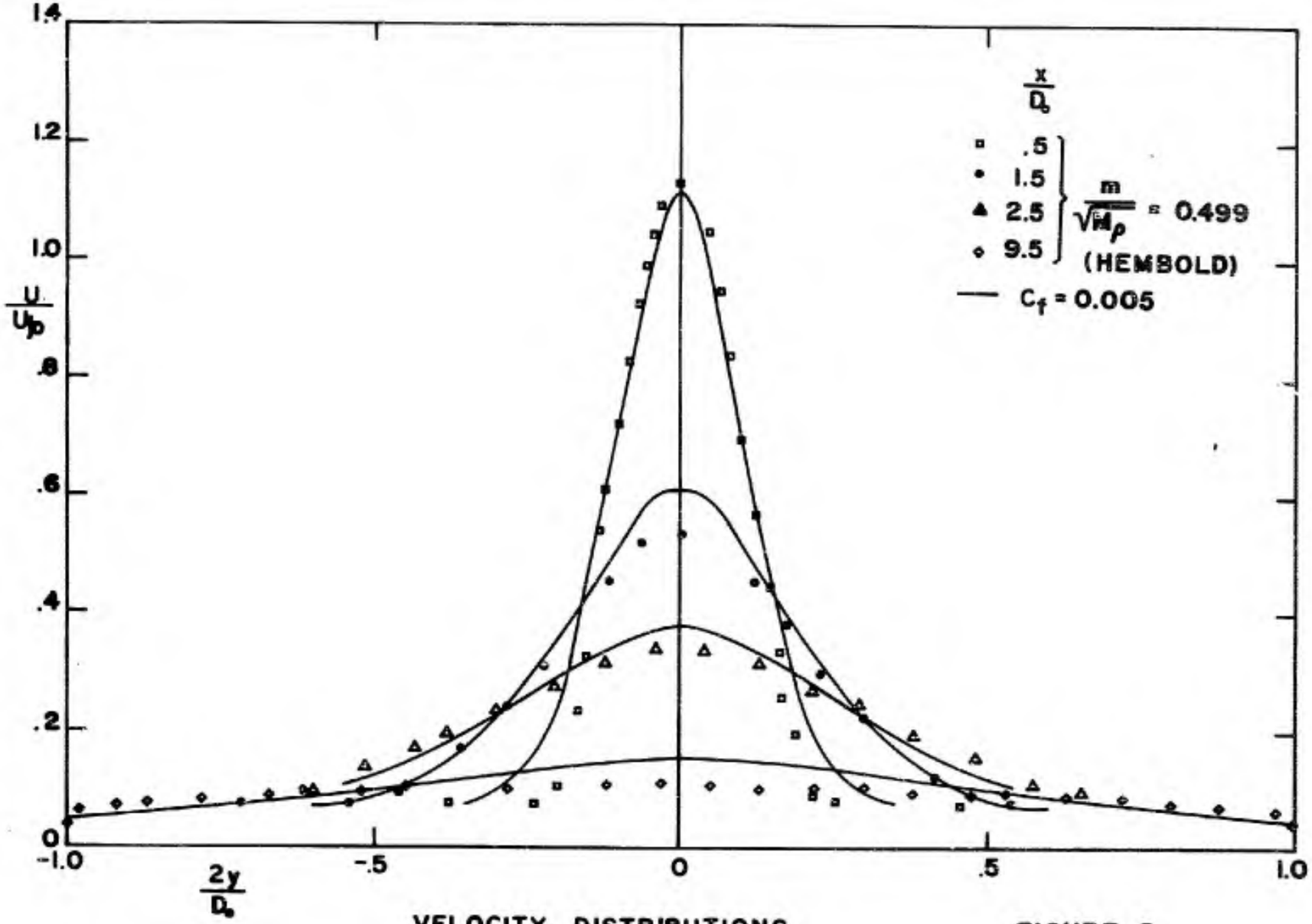

VELOCITY DISTRIBUTIONS

FIGURE 6

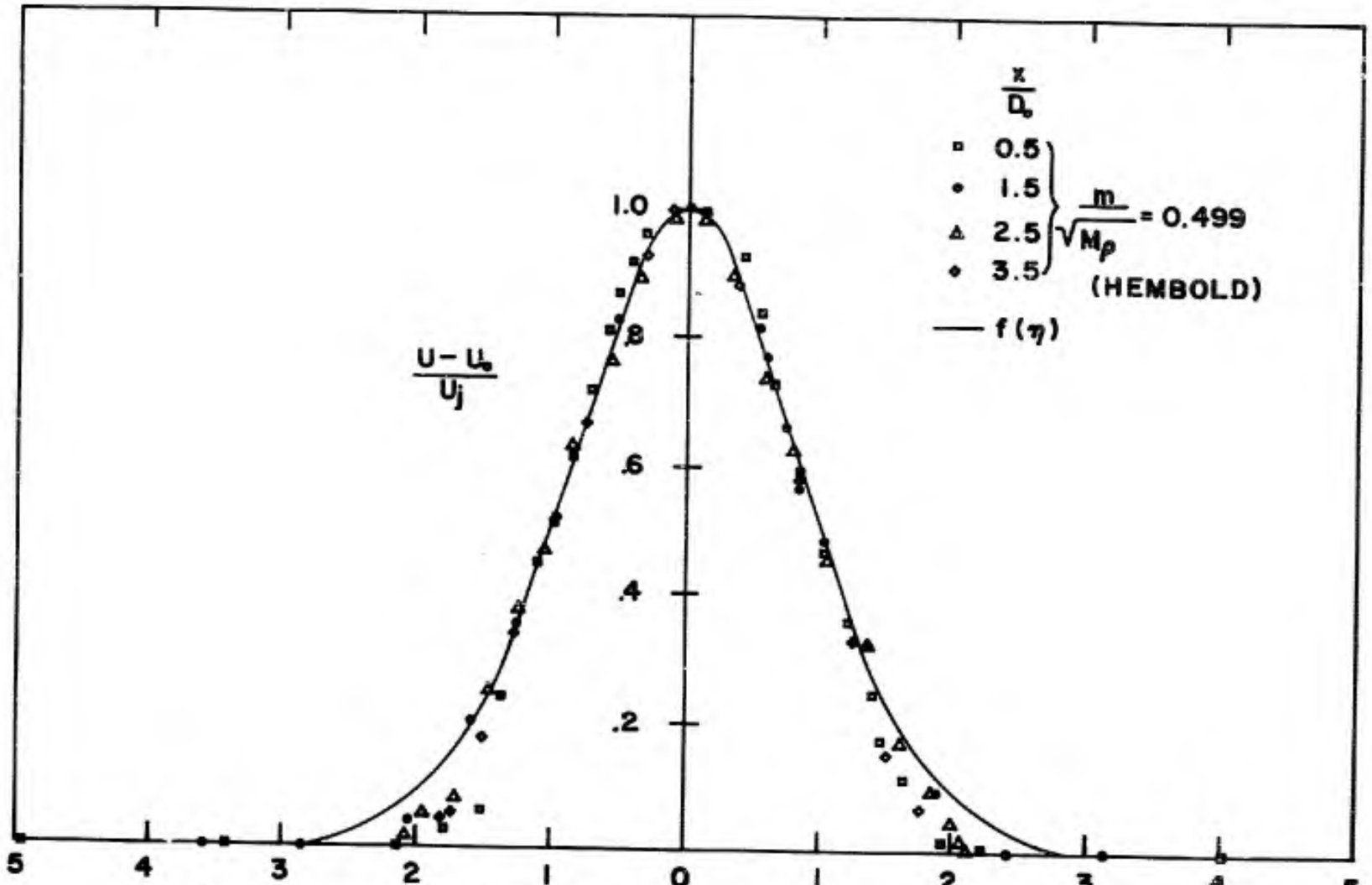

VELOCITY PROFILES

FIGURE 7

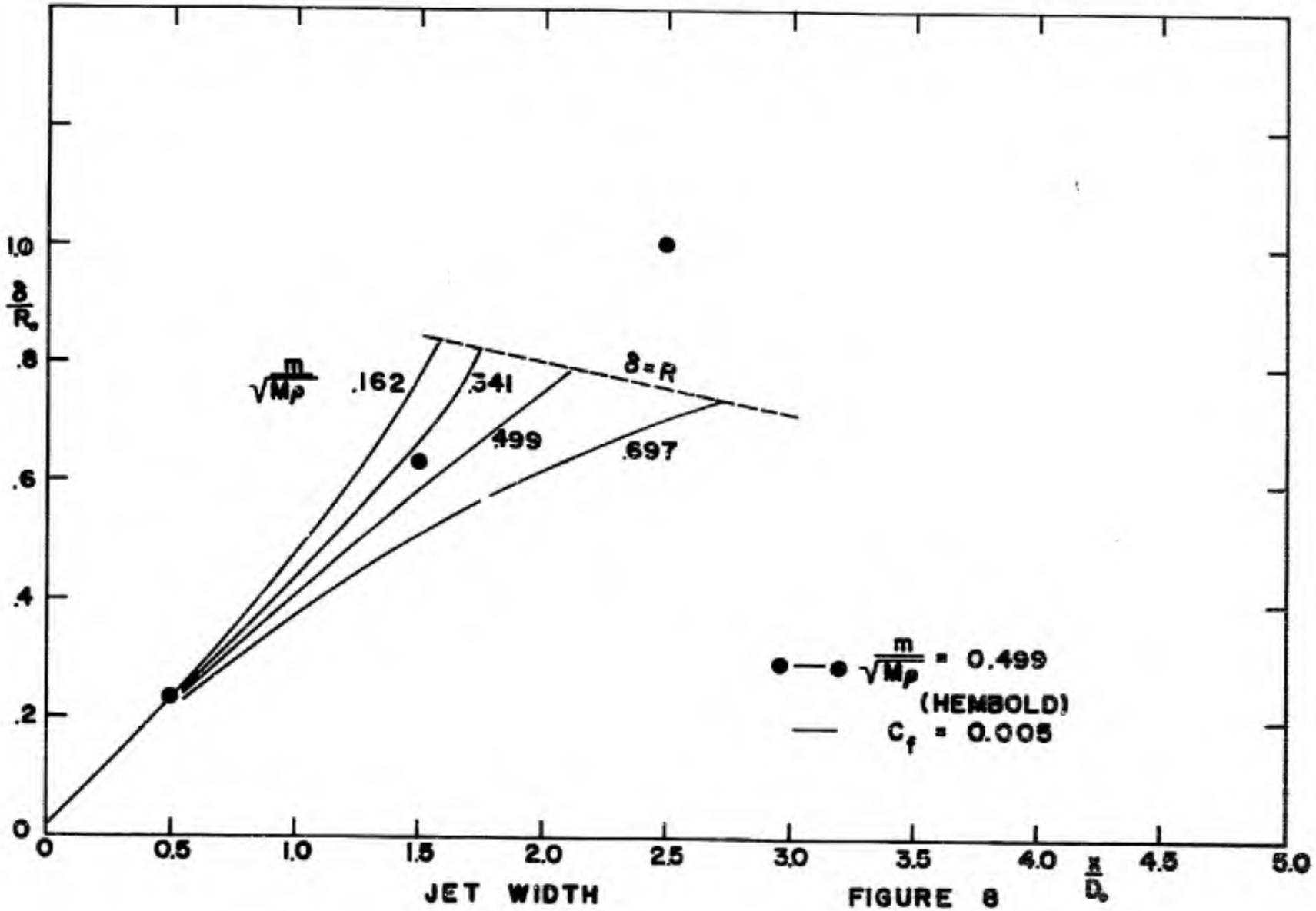
1.0
.8
.6
.4
.2
0
δ/R₀
m/√Mp .162
.341
.499
.697
δ=R
0
0.5
1.0
1.5
2.0
2.5
3.0
3.5
4.0
4.5
5.0
x/D₀
JET WIDTH
m/√Mp = 0.499
(HEMBOLD)
Cf = 0.005

FIGURE 8

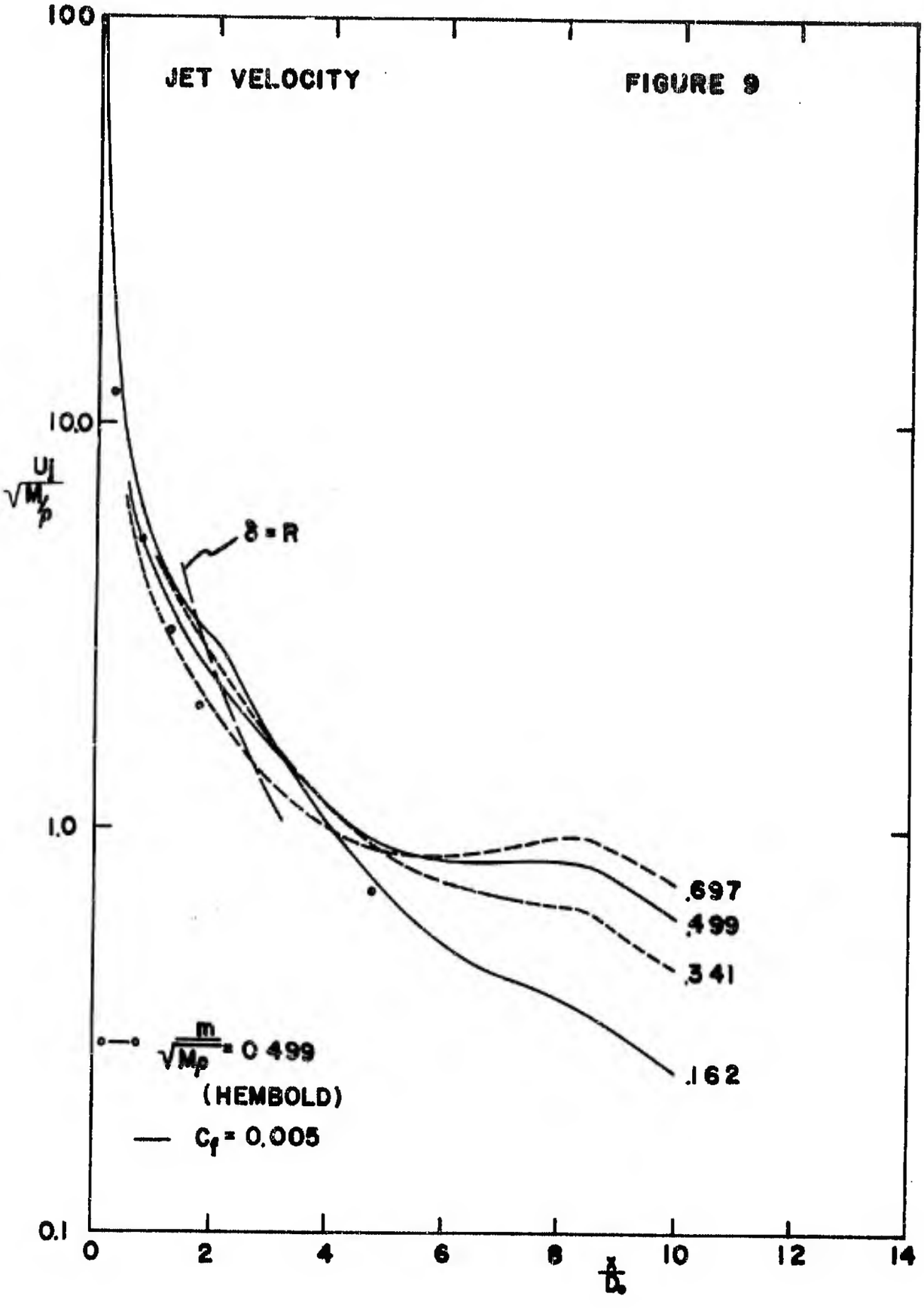
JET VELOCITY
FIGURE 9
100
10.0
1.0
0.1
$\frac{U_1}{\sqrt{M_p}}$
δ = R
.697
.499
.341
.162
$\frac{m}{\sqrt{M_p}}$ = 0.499
(HEMBOLD)
C_f = 0.005
0
2
4
6
8
10
12
14
$\frac{x}{D_e}$

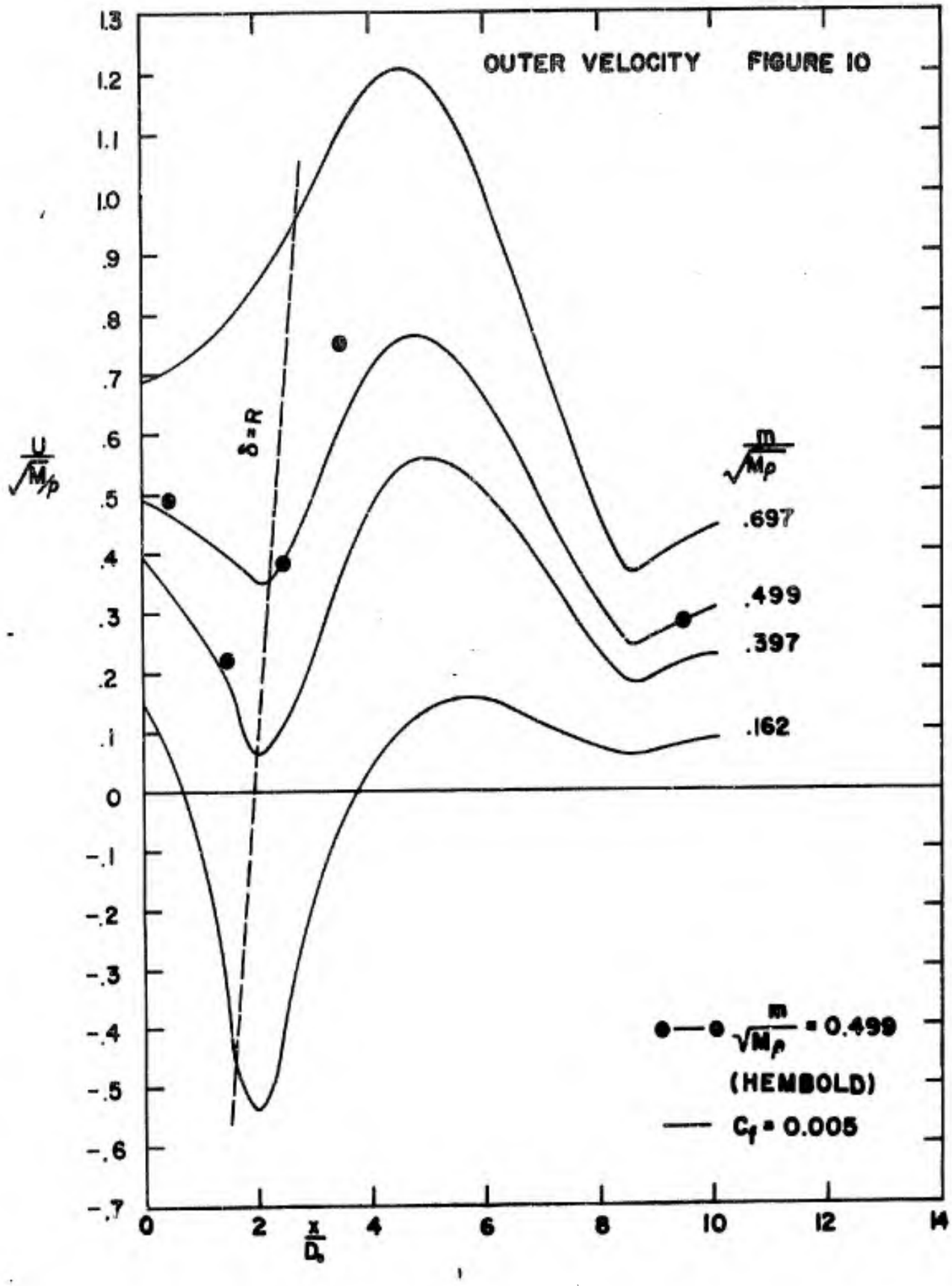
OUTER VELOCITY FIGURE 10
1.3
1.2
1.1
1.0
.9
.8
.7
.6
.5
.4
.3
.2
.1
0
-.1
-.2
-.3
-.4
-.5
-.6
-.7
0
2
4
6
8
10
12
14
$\frac{U}{\sqrt{M_p}}$
$\frac{x}{D_0}$
$\delta = R$
$\frac{m}{\sqrt{M_p}}$
.697
.499
.397
.162
$\frac{m}{\sqrt{M_p}} = 0.499$
(HEMBOLD)
$C_f = 0.005$

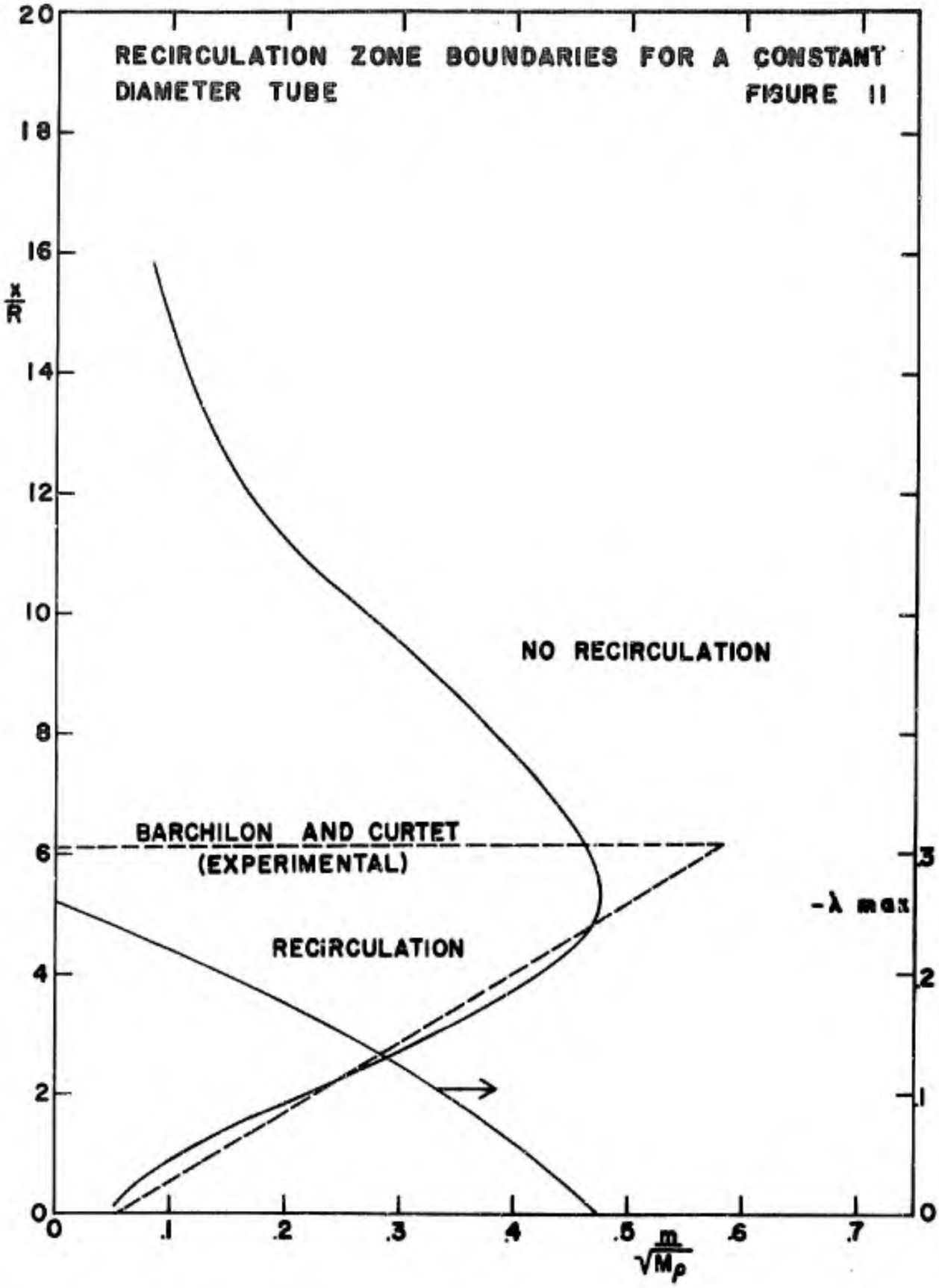
RECIRCULATION ZONE BOUNDARIES FOR A CONSTANT DIAMETER TUBE
FIGURE 11
x/R
NO RECIRCULATION
BARCHILON AND CURTET
(EXPERIMENTAL)
RECIRCULATION
-λ max
m/√Mρ
0
.1
.2
.3
.4
.5
.6
.7
2
4
6
8
10
12
14
16
18
20
1
3

RECIRCULATION IN A CONSTANT DIAMETER TUBE FIGURE 12

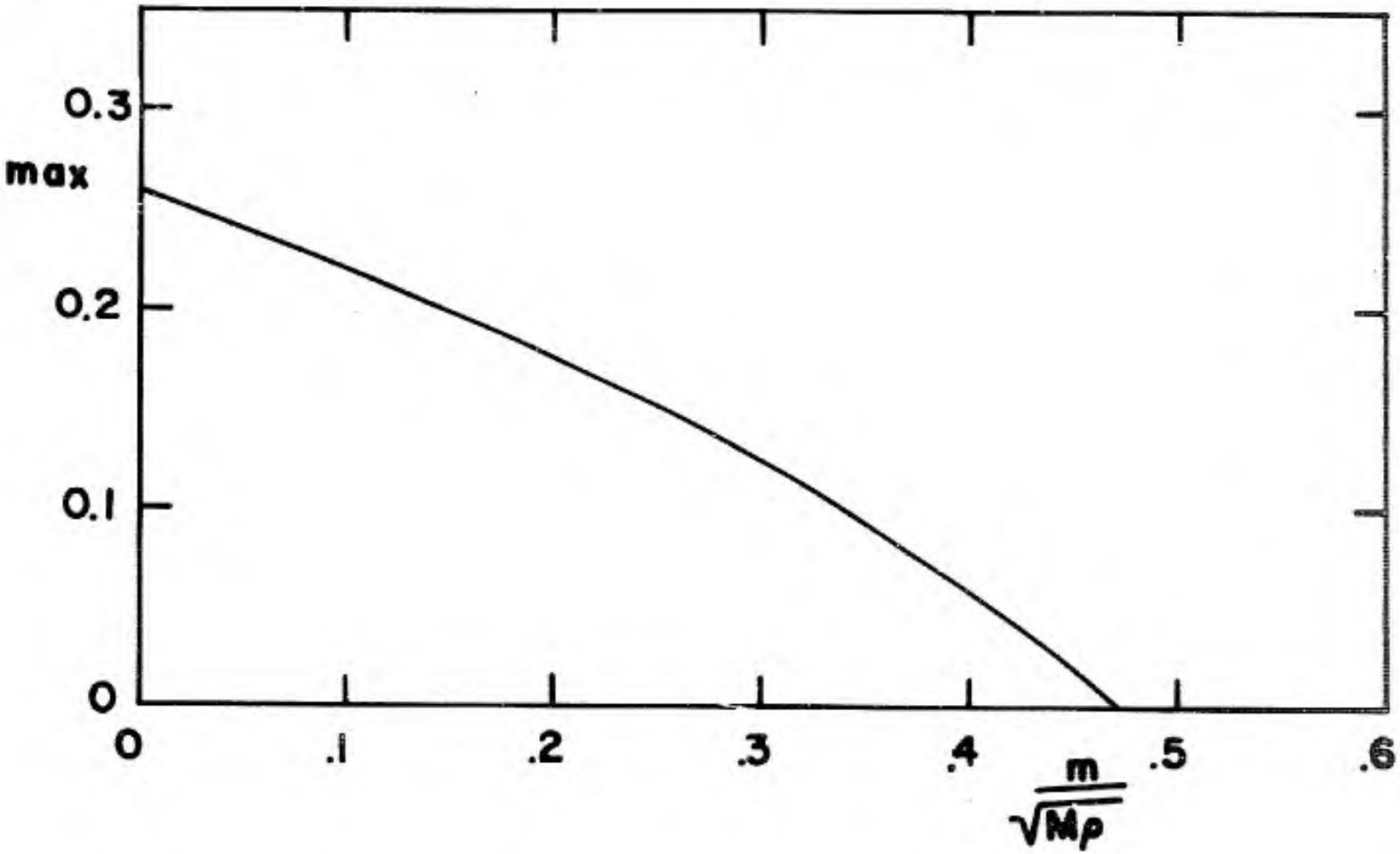

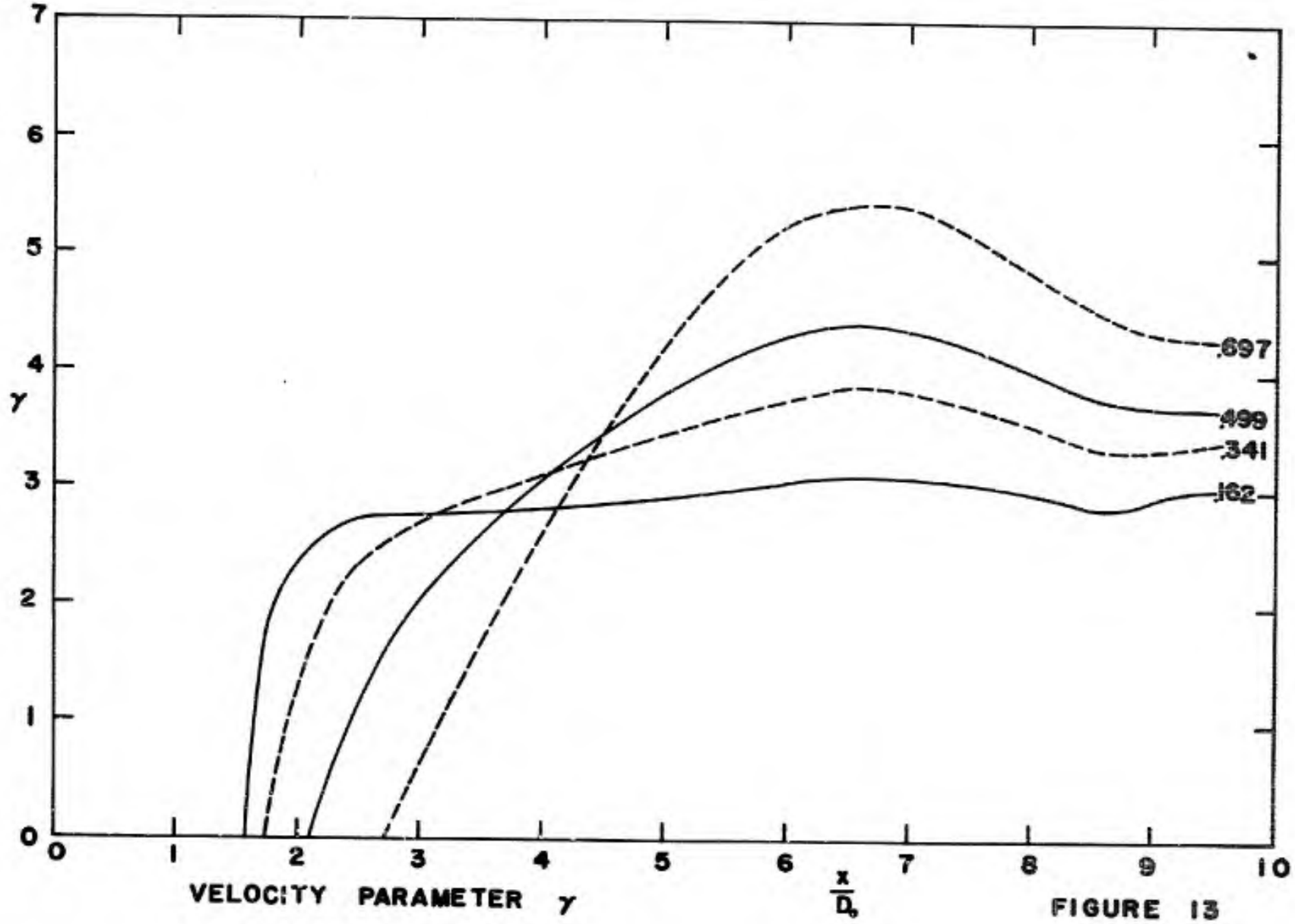
7
6
5
4
3
2
1
0
γ
0
1
2
3
4
5
6
7
8
9
10
.697
.499
.341
.162
VELOCITY PARAMETER γ
x/D₀

FIGURE 13

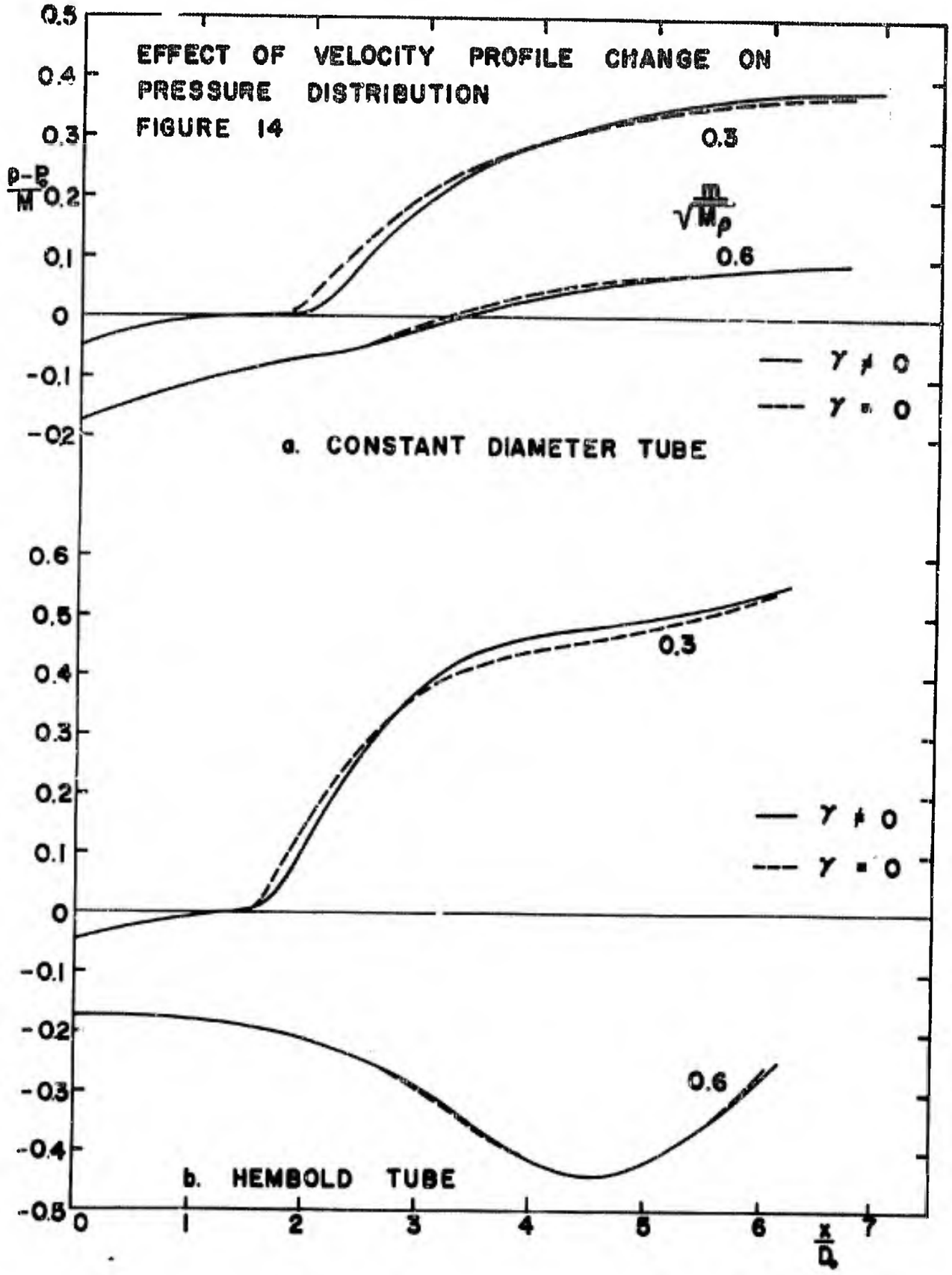
EFFECT OF VELOCITY PROFILE CHANGE ON PRESSURE DISTRIBUTION
FIGURE 14
$\frac{p-p_0}{M}$
$\frac{m}{\sqrt{M_p}}$
0.3
0.6
$\gamma \neq 0$
$\gamma = 0$
a. CONSTANT DIAMETER TUBE
b. HEMBOLD TUBE
$\frac{x}{D}$